The sensitivity of landfast sea ice to atmospheric forcing in single-column model simulations: a case study at Zhongshan Station, Antarctica

Fengguan Gu[1], Qinghua Yang[1], Frank Kauker[2,3], Changwei Liu[1], Guanghua Hao[4],

Chao-yuan Yang[1], Jiping Liu[5], Petra Heil[6], Xuewei Li[1], Bo Han[1*]

1 School of Atmospheric Sciences, Sun Yat-sen University, and Southern Marine Science and Engineering

Guangdong Laboratory (Zhuhai), Zhuhai 519082, China

2 Alfred Wegener Institute, Helmholtz Centre for Polar and Marine Research, Am Handelshafen 12, 27570

Bremerhaven, Germany

3 Ocean Atmosphere Systems, Tewesstseg 4, 20249 Hamburg, Germany

4 Key Laboratory of Marine Hazards Forecasting, National Marine Environmental Forecasting Center, Ministry of

Natural Resources, Beijing 100081, China

5 Department of Atmospheric and Environmental Sciences, State University of New York at Albany, Albany, NY,

USA

6 Australian Antarctic Division and Australian Antarctic Program Partnership, Private Bag 80, Hobart, Tas 7001,

Australia

Correspondence to: Bo Han (hanb5@mail.sysu.edu.cn)

Abstract

Single-column sea ice models are used to focus on the thermodynamic evolution of the ice. Generally, these models are forced by atmospheric reanalysis in the absence of atmospheric *in situ* observations. Here we assess the sea ice thickness (SIT) simulated by a single-column model (ICEPACK) with *in situ* observations obtained off Zhongshan Station for the austral winter of 2016. In the reanalysis, the surface air temperature is about 1 ℃ lower, the total precipitation is about 2 mm day^{-1} larger, and the surface wind speed is about 2 m s^{-1} higher compared to the *in situ* observations, respectively. We designed sensitivity experiments to evaluate the simulation bias in sea ice thickness due to the uncertainty in the individual atmospheric forcing variables. Our results show that the unrealistic precipitation in the reanalysis leads to a bias of 14.5 cm in sea ice thickness and 17.3 cm in snow depth. In addition, our data show that increasing snow depth works to gradually

inhibit the growth of sea ice associated with thermal blanketing by the snow due to changing the vertical heat flux. Conversely, given suitable conditions, the sea ice thickness may grow suddenly when the snow load gives rise to flooding and leads to snow-ice formation. Shortcomings of this simulation study are also discussed.

A potential mechanism to explain the different characteristics of the precipitation bias on snow and sea ice is discussed. The flooding process might cause different effects in landfast sea ice compared to pack ice, but ICEPACK has not distinguished.

1 Introduction

Sea ice plays an essential role in the global climate system by reflecting solar radiation and regulating the heat, moisture, and gas exchanges between the ocean and the atmosphere. In contrast to the rapid decline of sea ice extent and volume in the Arctic (Stroeve et al., 2012; Lindsay and Schweiger, 2015), satellite observations show a slight increase in the yearly-mean area of Antarctic sea ice since the late 1970s (Parkinson and Cavalieri, 2012) followed by a rapid decline from 2014 (Parkinson, 2019) and a renewed increase in most recent years (Chemke and Polvani, 2020). Although the sudden decline of Antarctic sea ice is yet to be attributed (Parkinson, 2019), the spatial pattern of Antarctic sea ice changes is suggested to be primarily caused by changes in the atmospheric forcing. For example, the rapid ice retreat in the Weddell Sea from 2015 to 2017 has been associated with the intensification of northerly wind (Turner et al., 2017), while the phase of the southern annular mode (SAM) significantly modulates the sea ice in the Ross Sea and elsewhere, especially in November 2016 (Stuecker et al., 2017; Schlosser et al., 2018; Wang et al., 2019a).

Landfast sea ice, the immobile fraction of the sea ice, is mainly located in near coastal regions of Antarctica, and its change is assumed to be indicative of the evolution of total Antarctic sea ice (Heil et al., 1996; Heil, 2006; Lei et al., 2010; Yang et al., 2016a). Unlike drifting sea ice, the change in landfast sea ice is dominated by thermodynamic processes, which single-column sea-ice models can well capture (Heil et al., 1996; Lei et al., 2010; Yang et al., 2016b; Zhao et al., 2017; Liu et al., 2022). Furthermore, a single-column sea ice model is a useful tool to evaluate the impacts of different atmospheric forcings on the sea ice evolution because of the relatively simple structure of the physical processes (Cheng et al., 2013; Wang et al., 2019b; Merkouriadi et al., 2020). In this study, a state-of-the-art single-column sea ice model, ICEPACK, is chosen to investigate the

sensitivity of landfast sea ice to atmospheric forcing for the region off Zhongshan Station in Prydz

Bay, East Antarctica (Figure 1).

Due to the lack of *in situ* observation, the majority of sea ice studies, especially for the Antarctic,

rely on numerical models. Realistic atmospheric forcing is critical for reliable model simulations.

Although being criticized for significant deviations from *in situ* observations (Bromwich et al., 2007;

Vancoppenolle et al., 2011; Wang et al., 2016; Barthélemy et al., 2018), atmospheric reanalysis data

are assumed to offer reasonable atmospheric forcing for large-scale sea ice models for the Antarctic

(Zhang, 2007; Massonnet et al., 2011; Zhang, 2014; Barthélemy et al., 2018). Previous studies

reported a large spread between four global atmospheric reanalysis products and *in situ* observations

in the Amundsen Sea Embayment (Jones et al., 2016). Moreover, studies showed that directly using

atmospheric reanalysis as forcing for models causes significant biases in the Arctic sea ice

simulations (Lindsay et al., 2014; Wang et al., 2019b). Similar results, accentuated by the sparseness

of atmospheric observations entering the reanalysis, can be foreseen for Antarctica. Therefore, the

atmospheric forcing needs to be evaluated carefully before simulating Antarctic sea ice. To our

knowledge, few studies have given a quantitative evaluation of the effect of different atmospheric

forces on sea ice simulations in Antarctica.

The coastal landfast sea ice in Prydz Bay is generally first-year ice. It usually fractures and is

exported or melts out completely between December and the following February, and refreeze

occurs from late February onwards (Lei et al., 2010). This seasonal cycle is representative of

Antarctic landfast sea ice. This study aims to evaluate the contributions of the various atmospheric

forcing variables on landfast sea ice growth. The snow cover exerts influence on the evolution of

the vertical sea ice-snow column via a number of mechanisms, including the formation of snow-ice

added by flooding (Leppäranta, 1983), superimposed ice (Kawamura et al., 1997), and insulating

impact (Massom et al., 2001). Understanding the snow depth is a primary concern here.

Two sets of atmospheric forcing have been chosen. The first is spatially interpolated ERA5 onto

the location of the observation site, and the second is using *in situ* atmospheric observations. It is

well-known that the simulation biases of numerical models are introduced through many

shortcomings, including unrealistic surface boundary conditions (here: atmospheric forcing),

imperfect physical process formulations, computational errors. Understanding the uncertainty in sea

ice simulations as well as the sea ice response pattern to atmospheric forcing due to imperfect

90   surface boundaries is a prerequisite for successful simulations and needs to be assessed first.

91   This study is arranged as follows: Section 2 introduces the *in situ* observations, the numerical

92   model, and the reanalysis. The main results are given in section 3, focusing on different kinds of

93   atmospheric forcing on sea ice and snow. Shortcomings, discussions and conclusions follow in

94   sections 4, 5 and 6.

95

96   **2 Materials and methods**

97   **2.1 Meteorological observations**

98   The site of sea ice observation ~~is~~ locates in the coastal area off Zhongshan Station

99   [(69°22′S,76°22′E); Figure 1], East Antarctica. The meteorological data were collected at a year-

100 round manned weather observatory run at Zhongshan Station in 2016, which is 1 km inland from

101 the sea ice observation site and 15 m above sea level. Snowfall is measured every 12 hours at the

102 Russian Progress II station (located ∼1 km to the southeast of Zhongshan Station). The short- and

103 long-wave radiation fluxes were measured every minute with a net radiometer mounted 1.5 m above

104 the surface on a tripod (Yang et al., 2016a). Other meteorological variables are available as hourly

105 data, including 2 m air temperature (T_{2m}), surface pressure (P_a), specific humidity (calculated from

106 dew-point temperature and P_a), potential temperature (calculated from T_{2m} and P_a), air density

107 (calculated by T_{2m} and P_a) and 10 m wind speed (U_{10}) (Hao et al., 2019; Hao et al., 2020; Liu et al.,

108 2020).

109
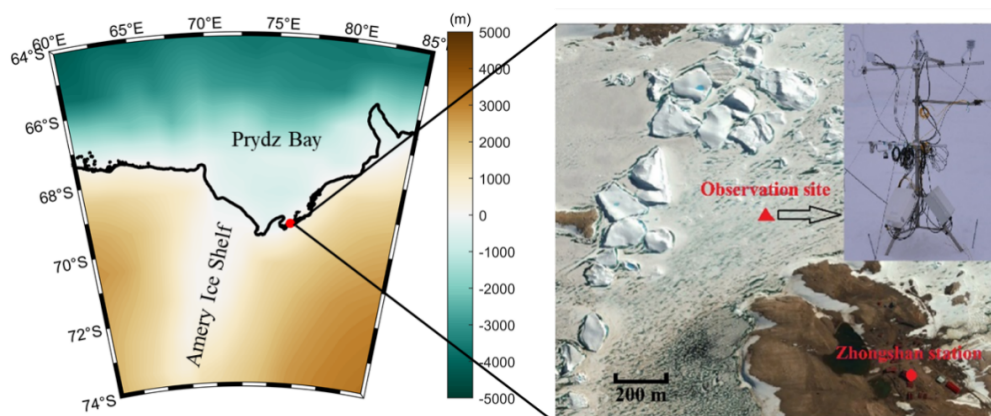
111 Figure 1 Location of landfast sea ice surface measurements near Zhongshan Station. The solid

112 triangle denotes the observation site, the solid circle marks Zhongshan Station. The color on the left

113 represents the terrain.

114

2.2 Sea ice thickness measurement

116 A thermistor-chain unit developed by Taiyuan University of Technology (TY) was used to
117 measure sea ice thickness in austral winter 2016. This unit is composed of two parts: the control unit
118 and the thermistor chain. The controller initiates data acquisitions and records and stores the
119 temperature measurements. The thermistor chain is 3 m long with 250 equidistant thermistors. Their
120 sensitivity is 0.063 ℃, and the measurement accuracy is ~~better than~~ ±0.1~~5~~ ℃. The thermistor chain
121 simultaneously records the vertical temperature profile across the near-surface atmosphere, snow
122 cover, sea ice, and surface seawater. The measurement frequency is hourly. Details about the
123 instruments can be found in Hao et al. (2019).

124 Snow thickness close to the thermistor unit is measured weekly using a ruler with an accuracy
125 of ±0.2 cm. Sea ice thickness is measured with a ruler through a drill hole (5 cm diameter) weekly.
126 The measurement accuracy is ±0.5 cm. The average thickness obtained from three close-by sites is
127 retained. Sea-surface temperature and sea-surface salinity are measured in the drill holes weekly
128 using a Cond 3210 set 1 (Hao et al., 2019).

129

2.3 Atmospheric reanalysis data

131 The European Centre for Medium-range Weather Forecasts (ECMWF) released ERA5, the new
132 reanalysis product in 2017, updated in near real-time (Hersbach and Dee, 2016; Hersbach et al.,
133 2020). The complete ERA5 dataset, extending back to 1950, has been available to the end of 2019
134 during this study. Compared with the popular ERA-Interim reanalysis, there are several significant
135 improvements in ERA5, including much higher resolutions (both spatially and temporally). ERA5
136 has global coverage with a horizontal resolution of 31 km by 31 km at the equator and 10 km by 31
137 km at the latitude of Zhongshan Station. The ERA5 resolves the vertical atmosphere profile using
138 137 vertical pressure levels from the surface up to a geopotential height of 0.01 hPa. ERA5 provides
139 hourly analysis and forecast fields and applies a four-dimensional variational data assimilation
140 system (4D-var). ERA5 includes various reprocessed quality-controlled data sets, for example, the
141 reprocessed version of the Ocean and Sea Ice Satellite Application Facilities (OSI SAF) sea ice
142 concentration (Hersbach and Dee, 2016; Hersbach et al., 2020).

For comparison and evaluation against the observation in this study, gridded data from ERA5 has been bilinearly interpolated to the observation site (detailed in 2.1). Directly using atmospheric forcing from coarse grid cells to interpolate to the observation site, although widely accepted in the previous studies (e.g., Urraca et al., 2018; Wang et al., 2019b), may cause errors. We have checked the performance of ERA5 and found that the spatial difference of surface atmospheric variables around the observation site is relatively small, indicating the choice of interpolation techniques will not affect the conclusion of this study.

2.4 ICEPACK

ICEPACK is a column-physics component of the Los Alamos Sea Ice Model (CICE) V6 and is maintained by the CICE Consortium. ICEPACK incorporates column-based physical processes that affect the area and thickness of sea ice. It includes several options for simulating sea ice thermodynamics, mechanical redistribution (ridging), and associated area and thickness changes. In addition, the model supports several tracers, including ice thickness, enthalpy, ice age, first-year ice area, deformed ice area and volume, melt ponds, and biogeochemistry (Hunke et al., 2019). ICEPACK Version 1.1.1 was used in this study, and detailed options of physical parameterizations and model settings for the ICEPACK are summarized in Table 1. We employ ICEPACK to distribute the initial ice thickness to each ice thickness category using a distribution function:

$$p_i = \frac{max\left(2 \times h \times H_i - H_i^2, 0\right)}{\sum_i max\left(2 \times h \times H_i - H_i^2, 0\right)}, \quad i = 1 \cdots N, \ (1)$$

Where h is the initial ice thickness, H_i is the prescribed ice thickness category (0–0.6, 0.6–1.4, 1.4–2.4, 2.4–3.6, and above 3.6 m~; same as for Arctic simulations), N is the number of ice thickness categories.

Table 1 Detailed options of physical parameterizations and model settings for the ICEPACK.

ICEPACK	Value
time step	3600 s
Number of layers in the ice	7
Number of layers in the snow	1
Ice thickness categories	5 (Bitz et al., 2001)
Initial ice thickness	99.5 cm (observed)
Initial snow depth	11.5 cm (observed)
Albedo scheme	CCSM3 (Collins et al., 2006)
Ice thermodynamic	Mushy-layer (Turner et al., 2013)
Shortwave radiation	Delta-Eddington (Briegleb and Light, 2007)

Snowdrift	Not implemented in ICEPACK 1.1.1
Melt ponds (superimposed ice)	Not used in this study
Ocean heat transfer coefficient	0.006 (Maykut and McPhee, 1995)
SSTst restoring time scale (days)	0 (use observed sst SST as oceanic forcing)
Minimum value of Oocean friction velocity minimum (m/s)	0.0005 (Tsamados et al., 2013)

166   The atmospheric forcing for the ICEPACK model consists of observations of downward short-

167 and long-wave radiation, 2 m air temperature, specific humidity, total precipitation, potential

168 temperature, 2 m air density, and 10 m wind speed. The oceanic forcing includes sea surface

169 temperature, sea surface salinity, and oceanic mixed layer depth. The period concerned in this study

170 is from April 22, when observed sea ice generally starts to grow, to November 22 in, 2016. Since

171 there are no observations of the ocean's mixed-layer depth, we set it to 10 m based on a previously

172 published study (Zhao et al., 2019).

173

174 **3 Results**

175   **3.1 Surface atmospheric conditions near the observation site**

176   First, we compare the eight atmospheric variables used to force ICEPACK (surface downward

177 shortwave radiation (R_{sd}), surface downward long-wave radiation (R_{ld}), surface air temperature (T_a),

178 specific humidity (Q_a), precipitation (P), air potential temperature (Θ_a), air density (ρ_a), wind speed

179 (U_a) with the respective *in situ* observation. Table 2 lists the bias (simulation reanalysis minus

180 observation), bias ratio (ratio between the bias and the observation value), the mean value of the *in*

181 *situ* observation (Mean_Obs), the correlation coefficient (Corr.), and the root-mean-square deviation

182 (RMSD) between the interpolated ERA5 data and the observation. In general, all eight variables

183 from the two sources closely follow each other (Corr. > 0.85), except for P and U_a. In this study, the

184 main attention is on the atmospheric variables T_a, P, and U_a for three reasons: (1) Previous studies

185 have shown that from all atmospheric forcing variables, uncertainties in T_a, P, and U_a exert a

186 significant impact on the sea ice thickness (Cheng et al., 2008). (2) Surface wind may affect the

187 snow cover in two ways: sublimation due to surface turbulent heat flux (Fairall et al., 2003; Gascoin

188 et al., 2013) and the snowdrift process (Thiery et al., 2012). (3) P and U_a from the reanalysis have

189 the largest bias ratio compared to the *in situ* observations.

190   The timing of daily variations of T_a is well represented by ERA5, especially for strong cooling

191 events (Figure 2a). However, ERA5 tends to underestimate warm events by a few degrees as well

as cold events where differences exceeding 10 °C may occur (Figure 2d). During the entire observation period in 2016, T_a from ERA5 was 1.2168 °C lower than the *in situ* observation. Also, previous studies reported similar disagreement in T_a between observation and reanalysis in Antarctica (Bracegirdle and Marshall, 2012; Fréville et al., 2014). The cold bias of T_a in the reanalysis was suggested to be caused by the ice surface schemes that cannot accurately describe the ice-atmosphere interactions of strongly stable stratified boundary layers that are frequent in Antarctica.

Table 2 Comparison of atmospheric forcing between ERA5 reanalysis and *in situ* observations.

Variable	Bias	Bias ratio (%)	Mean_Obs	Corr	RMSD
R_{sd} (W m^{-2})	6.115	9.031	67.714	0.967	40.981
R_{ld} (W m^{-2})	-19.153	-9.672	198.023	0.869	28.753
T_a (K)	-1.168	-0.453	257.809	0.967	2.820
Q_a (10^{-4} kg kg^{-1})	-0.769	-9.326	8.247	0.950	1.987
P (mm day^{-1})	2.010	303.509	0.660	0.639	0.825
Θ_a (K)	0.290	0.112	259.437	0.965	2.609
ρ_a (kg m^{-3})	-0.021	-1.592	1.322	0.958	0.026
U_a (m s^{-1})	2.145	50.735	4.228	0.765	2.989

The reanalyzed variable with the largest bias ratio from the observation is the precipitation (Figure 2b). Hourly precipitation from ERA5 was accumulated into daily data and compared with the nearest available daily precipitation records from the Progress II station. The maximum daily mean precipitation can reach 19.1 mm day^{-1} (July 11, 2016), with an average of 0.66 mm day^{-1} from April 29 to November 22, 2016. While ERA5 captures the main precipitation events, it significantly overestimated the magnitude of precipitation events, especially in July. In this month, the mean precipitation rate from ERA5 is 5.83 mm day^{-1}, while the observed is only 1.42 mm day^{-1}. From April to November, the accumulated precipitation from ERA5 is about 300% larger than that in the *in situ* observations. Nevertheless, using precipitation from Progress II for Zhongshan Station may be questioned because of the distance of about 1 km to Zhongshan Station. Moreover, the snowdrift due to strong surface wind can affect the precipitation observation and the local accumulated snow mass, which may further cause a significant bias in snow depth between simulation and observation.

215

216
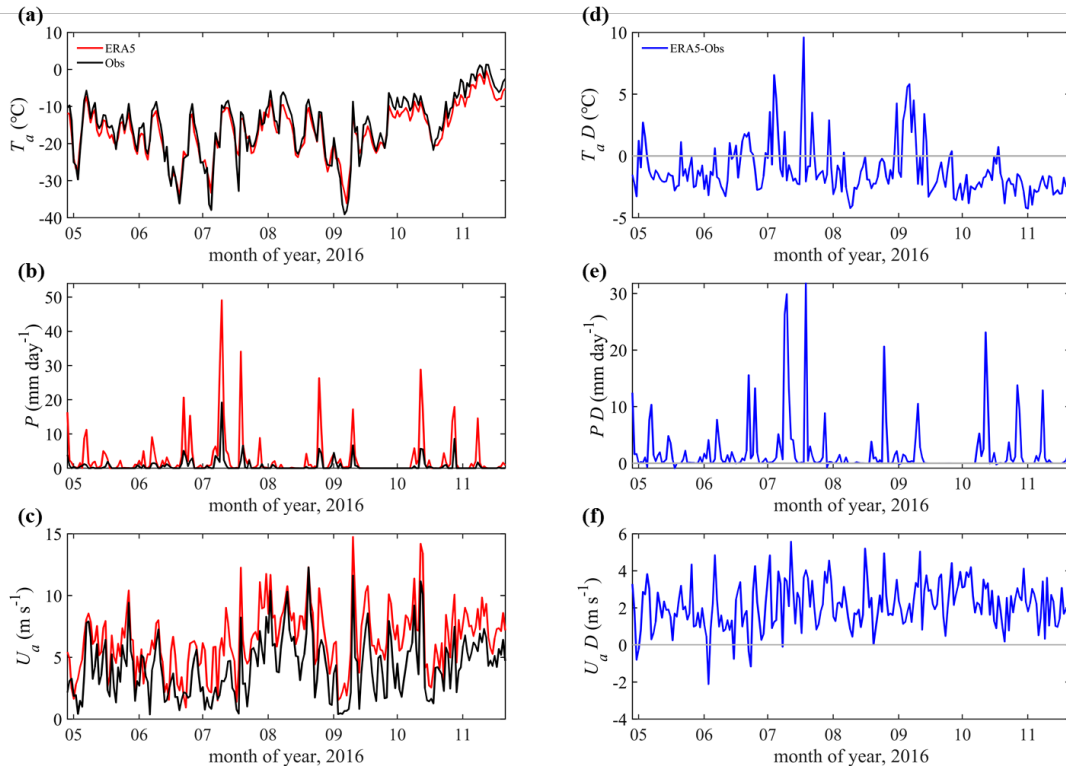
Figure 2 Time series of daily (a) surface air temperature, (b) precipitation rate, and (c) wind speed

(10 m above the surface). The ERA5 reanalysis data are indicated as red lines. Observations are

marked by black lines. (d-f) show the difference (marked by 'D') between ERA5 and the observation

(ERA5-observation). The differences are marked by blue lines. The gray lines denote the zero line.

221

The observed U_a varied from 0.01 m s^{-1} to 12.3 m s^{-1} with an average of 4.2 m s^{-1} (Figure 2c).

ERA5 well captured the daily and seasonal variation of U_a, but an overestimation of 2.1 m s^{-1} should

be noted, mainly when observed $U_a > 5$ m s^{-1}. One explanation for such overestimation is that the

numerical model underlying ERA5 cannot represent the surface roughness and the katabatic wind

in a region with complex orography (Tetzner et al., 2019; Vignon et al., 2019).

227

3.2 Simulation forced by observed *in situ* atmospheric variables

The simulation bias of sea ice thickness and snow depth is impacted by many aspects, including

unrealistic atmospheric and oceanic forcing and shortcomings in the applied numerical model. In

this study, we mainly focus on the influence of imperfect atmospheric forcing.

The sea ice thickness (Obs) measured through a hole drilled is increasing from April 29 (100±2

cm) to October 25 (172±2 cm), remaining level from there on (Figure 3a). The ice thickness deduced from the TY (Obs_TY) thermistor-chain buoy shows a similar result: sea ice thickness increased from 106 cm on April 22 to 171 cm on November 17. In November, the sea ice thickness (Obs and Obs_TY) is stationary, indicating a thermodynamic equilibrium between heat loss to the atmosphere and heat gain from the ocean (Yang et al., 2016a; Hao et al., 2019).

When forced by atmospheric *in situ* observations (Sim_Obs), the simulated sea ice thickness agrees well with the observed thickness with a mean bias of less than 1 cm over the growing season. We attribute the excellent simulation result to the fact that the seasonal evolution of landfast is driven mainly by thermal processes, which ICEPACK captures well.

The average snow depth from observation is 17 cm during the ice-growth season, with low snow depth measured before July 11 (Figure 3b). After that, the snow depth increases rapidly up to about 37 cm, associated with a precipitation event arising from a single synoptic system. Then it decreases below the seasonal mean (Obs_mean), followed by two secondary maxima (> 25 cm) on September 8 and October 18, respectively.

The snow depth in Sim_Obs tracks the observation closely before August 2 (Figure 3b). Then, the Observed snow depth decreased quickly from about 30 cm to about 10 cm, while the Sim_Obs snow depth continued to increase gradually until the onset of surface melting in November. We attribute the Observed quick decrease of snow depth to the effect of the snowdrift because the surface wind stayed above 5 m s^{-1} for most of August (Figure 2c), giving rise to snowdrift, a process not implemented in the version of ICEPACK used here. The snowdrift might cause a significant spatial difference in accumulated snow patterns (Liston et al., 2018), which may be responsible for the large deviation in snow depth between Sim_Obs and Observation. In addition, Sim_Obs underestimated the snow depth on July 11. As discussed above, using nonlocal observed precipitation from Progress II should be questioned.

Using observed meteorological variables as atmospheric forcing in ICEPACK produced unreliable snow depth while the sea ice thickness was in reasonably good agreement. In other words, the enormous bias in snow depth seems to have little effect on the sea ice thickness in the simulation. This counter-intuitive finding is of great interest to us because it disobeys the general realization that the snow layer significantly modifies the energy exchange on top of the sea ice. Potential causes for this result will be discussed later.

263

264
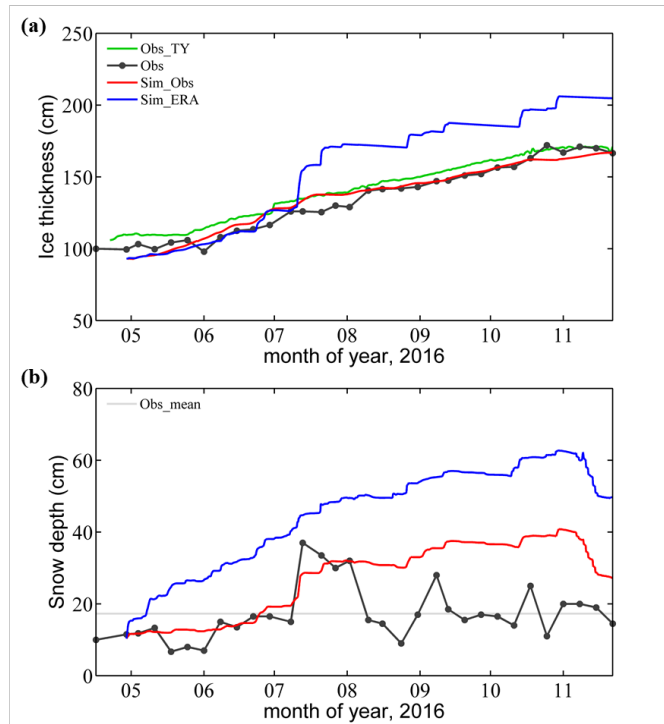
Figure 3 Time series of (a) sea ice thickness and (b) snow depth during the freezing season. Black

solid lines with black points show the observations from the drill hole (Obs). Green solid lines show

the ice thickness derived from the TY buoy (Obs_TY). Red solid lines show the simulation results

under *in situ* atmospheric forcing (Sim_Obs), and blue solid lines are simulation results under ERA5

forcing (Sim_ERA). In (b), the gray solid line shows the seasonal mean snow depth observation

(Obs_mean).

3.3 Simulation forced by ERA5 atmospheric variables

When forced by ERA5 (Sim_ERA), the simulated sea ice thickness shows significant deviations

from observation (Figure 3a). The deviation is only about 1 cm before July 11, when a heavy

precipitation event (~19 mm day^{-1}) happened. After the precipitation episode, the offset in the sea

ice thickness between Sim_ERA and observation was almost constant, about 33 cm.

In contrast to sea ice thickness, the precipitation from ERA5 causes an overestimation in snow

depth for the entire simulation period. The snow depth from Sim_ERA is much greater than

observation, even before July 11 (Figure 3b). During the heavy precipitation event (Figure 2b), the

observed snow depth increased from 20 cm to about 40 cm. Although the precipitation rate from

ERA5 (~40 mm day^{-1}) is two times larger than the observation, it caused little response in the simulated snow depth. The snow depth increase is near-linear, from about 10 cm to almost 60 cm.

3.4 Sensitivity analysis

To ~~find out which atmospheric variables including T_a, P and U_a are the most crucial in the sea ice simulation, a set of sensitivity simulation experiments is conducted~~determine which atmospheric variables, including T_a ~~Ta~~, P, and U_a ~~Ua~~, are the most crucial in the sea ice simulation, we designed a set of sensitivity simulation experiments, named SEN1. The simulation under the forcing from the *in situ* observed atmospheric variables is the control experiment and is named Sim_Obs. In each experiment of SEN1, one atmospheric variable is replaced by the corresponding variable from ERA5, while all others are identical to those of the control experiment. In Table 3, the averaged bias between the simulation and the observation of the outputs (ice thickness and snow depth), and ~~or~~ the bias ratio of forcing atmospheric variables~~,~~ are listed separately.

Table 3 Bias of ice thickness, snow depth, and bias ratio for each forcing variable come from Table 2. 'All' means using the full set of ERA5 atmospheric forcing.

Variable	Bias		Bias ratio (%)
	Ice (cm)	Snow (cm)	Forcing
R_{sd} (W m^{-2})	-0.044	-0.130	9.031
R_{ld} (W m^{-2})	3.050	2.243	-9.672
T_a (K)	0.001	0.029	-0.453
Q_a (10^{-4} kg kg^{-1})	1.099	-1.299	-9.326
P (mm day^{-1})	14.519	17.312	303.509
Θ_a (K)	-0.483	0.407	0.112
ρ_a (kg m^{-3})	0.119	-0.071	-1.592
U_a (m s^{-1})	-0.311	-3.421	50.735
All	16.824	17.882	/

~~The results from Sim_ERA are connected with the sensitivity of sea ice and snow depth to atmospheric forcing change.~~ To determine the sensitivity of sea ice and snow depth near Zhongshan station on atmospheric forcing, we designed a set of numerical experiments named SEN2~~1~~. In the control run, the forcing of the simulation directly used the means of observed atmospheric variables

302 (Mean_Obs in Table 43). For a specific atmospheric variable, we build a set of sensitive runs. The

303 focused atmospheric variable changed from its mean (Range in Table 34), and other variables are

304 the same as the control run. Considering the actual range ofin each observed variable on an

305 interannual scale (Van Den Broeke et al., 2004; Jakobs et al., 2020; Roussel et al., 2020), we set the

306 maximum change in T_a, Θ_a, and ρ_a to 2%, and other atmospheric variables to 50%. Then, we

307 concluded the sensitivity of sea ice and snow to each atmospheric forcing from its corresponding

308 sensitive runs. Because sea ice and snow depth show a quasi-linear response to the change in each

309 specific atmospheric forcing (not shown), the choice of the variable's range will not alter the

310 sensitivity results.

311

312 Table 43 The atmospheric forcing (Mean_obs for the control run and range for the sensitive run),
313 and sensitivity, and potential bias from SEN21.

Variable	Mean_Obs (Control)	Range (%)	Sensitivity	
			Ice (cm/%)	Snow (cm/%)
R_{sd} (W m^{-2})	67.714	±50	-0.033	-0.008
R_{ld} (W m^{-2})	198.023	±50	-0.368	-0.201
T_a (K)	257.809	±2	-1.247	-0.526
Q_a (10^{-4} kg kg^{-1})	8.247	±50	-0.025	0.029
P (mm day^{-1})	0.660	±50	-0.032	0.135
Θ_a (K)	259.437	±2	-1.297	-0.491
ρ_a (kg m^{-3})	1.322	±2	-0.054	0.021
U_a (m s^{-1})	4.228	±50	-0.054	-0.022

314

315 Comparing the individual biases in Table 3, it turns out that P and R_{ld} from ERA5 contribute to

316 the bias in sea ice thickness most strongly. For snow depth, P, U_a, and R_{ld} contribute the largest. In

317 Table 4, the sensitivity of ice thickness and snow depth to each atmospheric variable are listed.

318 Comparing the individual sensitivity, it turns out that the sea ice thickness and snow depth are most

319 sensitive to T_a and Θ_a. However, T_a from ERA5 is close to the *in situ* observation, so the simulated

320 sea ice thickness and snow depth isare hardly impacted (Table 3). The results from SEN1 reveal that

321 the overestimation in P in ERA5 is the majorprimary source forof the overestimation of sea ice

322 thickness and snow depth, even with less sensitivity to precipitation (Table 4).

323 In Table 3, the sensitivity of ice thickness and snow depth to each atmospheric variable are listed.

324 ~~Comparing the individual sensitivity, it turns out that the sea ice thickness and snow depth are most~~

325 ~~sensitive to T_a and Θ_a. However, since T_a and Θ_a from ERA5 is close to the *in situ* observation, the~~

326 ~~potential bias contributed by these two terms is relatively small. In contrast, the most significant~~

327 ~~overestimation in P in ERA5 is the primary source for the simulation bias for sea ice thickness and~~

328 ~~snow depth.~~

329   -To clarify the effect of specific forcing further, we replaced the x forcing in Sim_Obs with the

330   corresponding ERA5 variable and named it Sim_ERA_x. Compared with Sim_Obs, Sim_ERA_P

331   overestimates the snow depth since May (Figure 4b) and shows a significant positive bias in sea ice

332   thickness after July 11 (Figure 4a). Before July 11, the sea ice thickness from Sim_ERA_P was even

333   smaller than that from Sim_Obs.

334

335   To find out why the snow and sea ice behaves differently, we first investigate the net heat flux

336   into the ~~ice~~ snow surface H_N (positive downward):

337
$$H_N = Rn + Hs + Hl, (2)$$

338   where Rn, Hs, and Hl are the net surface radiation flux, the sensible heat flux, and the latent heat

339   flux, respectively. All energy fluxes are defined as positive downward. Because the simulated snow

340   layer in SIM_ERA_P is much deeper than in SIM_Obs, the difference ~~of~~ in H_N reflects the

341   modification of the surface energy flux due to the changed snow layer. From Figure 4d, it can be

342   deduced that the overestimation of snow depth in SIM_ERA_P results in a positive anomaly of H_N

343   before July 11, which hampers the sea ice growth. Later the difference ~~of~~ in H_N becomes relatively

344   small. The dependence of H_N on the snow depth is significant when the snow layer is shallow (<20

345   cm in this study). If the snow layer is deep enough, its impact on the net surface heat flux ceases.

346   After July 11, the difference in sea ice thickness between the two simulations increases quickly

347   from ~0 to >40 cm (Figure 4a). We attribute that to flooding with subsequent snow-ice formation

348   (Powell and others, 2005). The continuously deepening snow layer reduces the sea ice freeboard.

349   When heavy snowfall occurs, which frequently happens after July 11, the snow load pushes the sea

350   ice surface below sea level, and seawater floods onto the sea ice surface, causing the overlying snow

351   to freeze. This snow-ice formation process will form flooding ice (snow-ice thickness) at the sea ice

352   surface and rapidly increase the total sea ice thickness (Figure 4a). The difference (~100 cm) in

353   accumulated flooding ice (Figure 4c) between Sim_Obs (0.8 cm) and Sim_ERA_P (105.5 cm) is

much greater than the difference (~40 cm) in simulated sea ice thickness (Figure 4a), while the net

surface heat flux compares well after July 11 (Figure 4d). This difference may be because as the

snow-ice process occurs, the increase in sea ice thickness will reduce the heat loss from the ice

cover<s>transfer between the ocean and the atmosphere</s> and inhibit the basal growth of sea ice in winter

(Figure 4e). The flooding-induced snow-ice formation happens <s>with</s> at a rate larger than 0.5 cm per

hour after July 11. The snowfall (Figure 2b) is converted to new snow depth at the top surface

(Figure 4f) using a snow density of 330 kg m^{-3} in ICEPACK (Hunke et al., 2019). Comparing Figure

4b with Figure 4f, we find that the change in actual snow depth (11 cm) is much lower than the

expected accumulated snowfall (57 cm), indicating that the flooding process reduces about four-

fifths of snow depth over sea ice.
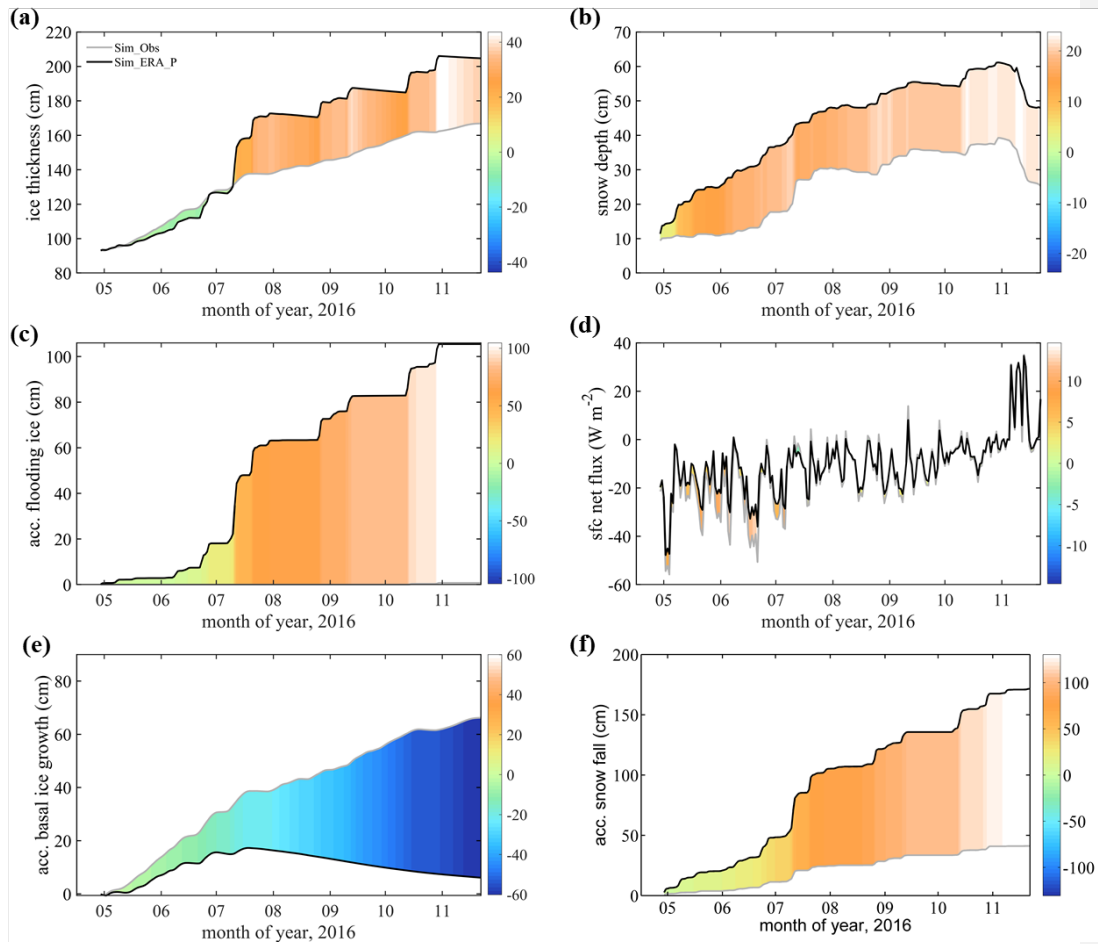
Figure 4 Times series of (a) sea ice thickness, (b) snow depth, (c) accumulated flooding ice, (d) net

surface heat flux, (e) accumulated basal ice growth, and (f) accumulated snowfall. The gray line

represents the simulation using precipitation from observation (Sim_Obs). The black line represents

369   the simulation using precipitation from ERA5 (Sim_ERA_P). The color bar represents their

370   difference (Sim_ERA_P – Sim_Obs).

371   **3.5 Additional sensitivity simulations on the precipitation bias**

372   The precipitation from ERA5 shows the most significant deviation compared to the *in situ*

373   observation and contributes the largest to the sea ice and snow simulation bias. To determine the

374   cause of differences in the sea ice and snow response to precipitation, we set up ten sensitivity

375   experiments named SEN32 (Figure 56). In the *n*-th experiment, *n*×10% of the daily difference

376   between *P* from ERA5 and the *in situ* observation is added to the observed *P* on that day. This

377   procedure gradually increases the magnitude of the precipitation in the experiments, while the

378   timing of the daily precipitation events remains almost unchanged.

379

380
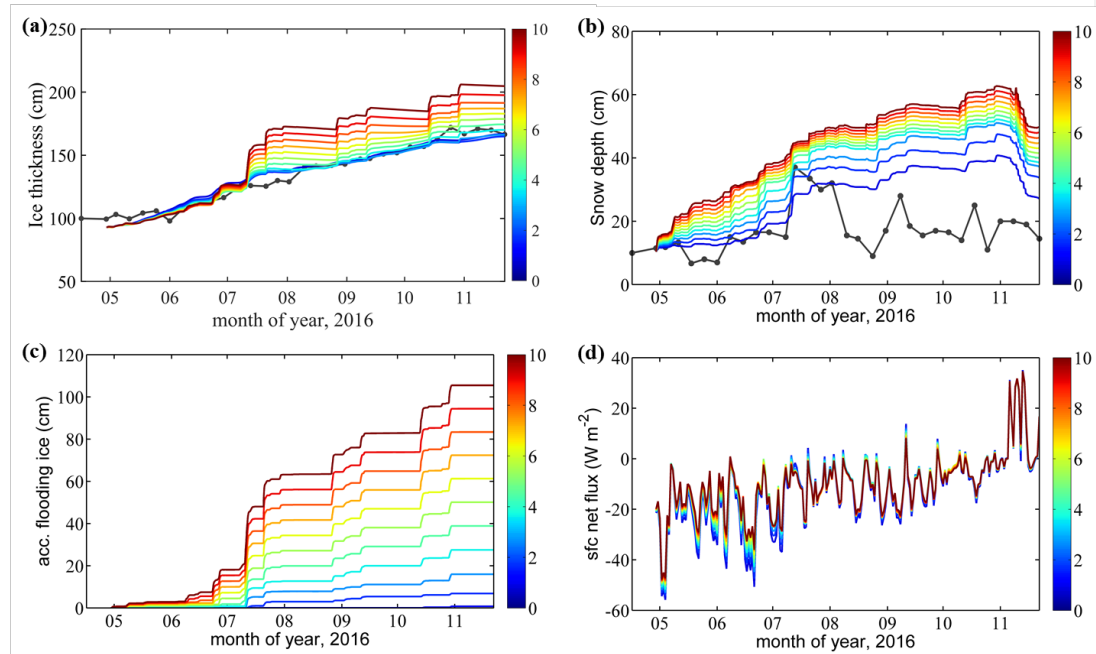
381   Figure 56 Time series of the simulated (a) sea ice thickness, (b) snow depth, (c) accumulated

382   flooding ice, and (d) net surface heat flux in the n experiments of SEN23. The black solid point lines

383   show the *in situ* observations (Obs). The 11 colored lines denote the 11 sensitivity experiments.

384   When *n* = 0, precipitation is from the *in situ* observation. When *n* = 10, precipitation is from ERA5.

385

386
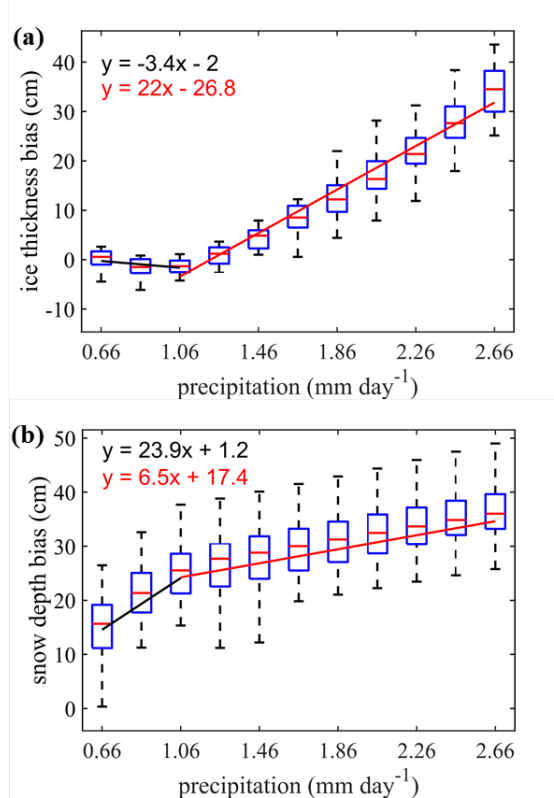
Figure 67 Box plot of simulation bias (simulation minus observation) of (a) sea ice thickness and
(b) snow depth over the daily mean precipitation in the different sensitivity experiments (n increases
from left to right). On the x-axis, 0.66 mm refers to the experiment with n=0 (*in situ* precipitation),
and 2.66 mm refers to the n=10 experiment (ERA5 precipitation). Two linear regression lines (black
and red) are derived for x <= 1.06 mm and x > 1.06 mm based on the mean of ice thickness and
snow depth.

We define the bias as the difference between simulations and observations from July 27 to the
end of November. Different start or end dates of this period do not change this result. The bias of
both sea ice thickness and snow depth linearly grows with increasing precipitation (Figure 67). The
simulation bias of the sea ice thickness is relatively small before the precipitation increases by about
1 mm per day. We suggested that the snow-ice formation is small (Figure 56c), and the insulation
of the snow layer (Figure 56d) hampers the sea ice growth. In fact, the simulated sea ice thickness
even decreases (at a rate of -3.4 cm/(mm day^{-1})) when the added precipitation is < 1 mm day^{-1}. When
the added precipitation is > 1 mm day^{-1}, the simulated sea ice thickness quickly increases at a rate
of 22 cm/(mm day^{-1}).

In contrast, the simulated snow depth increases ~~deepens~~ rapidly at 23.9 cm/(mm day^{-1}) when the

enforced precipitation remains small but at a rate of 6.5 cm when the added precipitation is large. This is because more snow is converted into flooding ice, and the snow-ice formation process strongly overrules the larger insulation effect from the snow layer, promoting sea ice growth.

The snow-ice process is based on Archimedes' Principle. Therefore, the threshold value (1 mm/day^{-1}) is related to the density value of ice, snow, and water in model parameterization as well as the sea ice thickness and snow depth. If sea ice and snow density, initial snow depth decrease, or seawater density and initial ice thickness increase, the threshold will increase, and vice versa. These different effects of increases in precipitation on the snow and sea ice growth are illustrated in Figure 78, emphasizing the role of flooding via snow-ice formation. When the snow layer is shallow, increases in precipitation will quickly deepen the snow layer and inhibit the growth of sea ice thickness due to the insulation of snow. The decrease in the surface net heat flux is the dominant factor. While the snow layer is deep and large precipitation is present, the flooding process induces snow-ice formation, and the sea ice grows quickly while the snow depth increases only slowly.
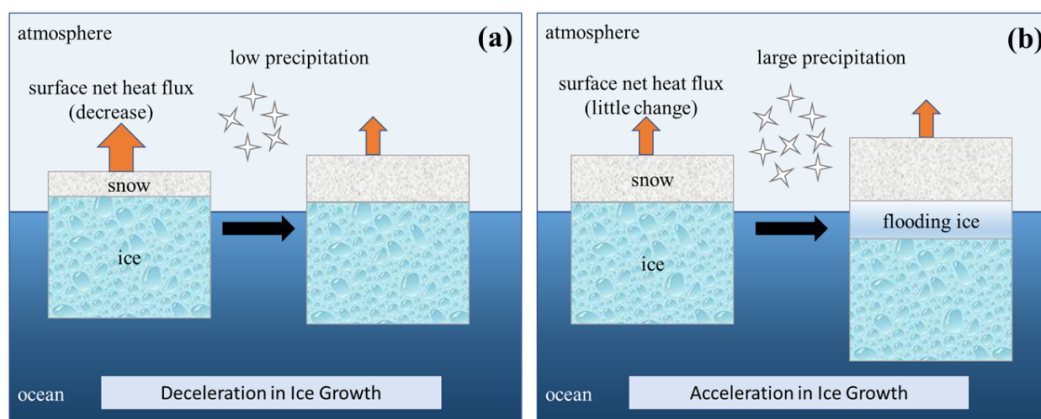
Figure 78 Schematic diagram for (a) low precipitation and (b) large precipitation events illustrating the precipitation effect on sea ice growth. The orange arrows represent surface net heat flux, and different colored boxes indicate the layer of snow, flooding ice, and sea ice.

4 Shortcomings

The simulated ice thickness and snow depth deviate from the observations in this study (Figure 3). We list the shortcomings that could affect the simulation: 1) Superimposed ice is not considered in this study; 2) TThe snow-ice formation might be overestimated on the landfast sea ice in ICEPACK; 3) The sSnowdrift process has not been involved in the version of ICEPACK used here.

428   Superimposed ice is present in early autumn when the snow starts to melt (Kawamura et al.,

429   1997) and contributes significantly to sea ice growth (up to 20% of mass) (Granskog et al., 2004).

430   Superimposed ice usually corresponds to liquid precipitation or melted snow that permeates

431   downward to form a fresh slush layer and refreezes. The superimposed ice is implemented in

432   ICEPACK via the melt ponds parametrization but has not been considered in this study ~~because the~~

433   ~~deformation information of sea ice is not available~~. Therefore, the simulation may underestimate

434   sea ice thickness and overestimate snow depth compared to the observation in November (Figure

435   3a). We will apply the melt ponds scheme in the follow-up research work.

436   ~~The snow-ice formation might be overestimated on the landfast sea ice in ICEPACK.~~ Flooding-

437   induced snow-ice formation is common in the Antarctic ocean because of the thin ice and heavy

438   snowfall (Kawamura et al., 1997). It can contribute to considerable ice mass (12%-36%) and reduce

439   the snow depth by up to 42-70%, depending on the season and location (Jeffries et al., 2001). The

440   parameterization of the flooding process in the ICEPACK is based on Archimedes' Principle for the

441   pack ice, which might be problematic for the coastal landfast sea ice. With a much larger volume

442   and shallower seawater around than the pack sea ice, part of the coastal landfast sea ice might contact

443   the sea bed rather than float in the sea. Thus, the flooding should be much weaker even with

444   weighted snow cover. Besides, the change in density of ice due to the flooding process is significant

445   (Saloranta, 2000) but not well considered in ICEPACK. For example, a slushy layer of 10 cm depth

446   would refreeze within three days from observation (Provost et al., 2017), while the process only

447   needs one day in ICEPACK. Hence, the landfast sea ice growth due to snow-ice formation needs

448   improvement in ICEPACK, especially when the input precipitation is significantly exaggerated, e.g.,

449   the ERA5 forcing.

450

451   **~~5 Discussions~~**

带格式的:
无, 缩进: 首
行缩进:
0.74 厘米

452   Surface drifting snow particles play an essential role in the surface mass balance (Van den

453   Broeke et al., 2004). Figure 3b shows that the observed snow depth has quickly decreased from 32

454   cm on August 2 to 15.5cm on August 10, which should be attributed to the snowdrift because the

455   surface wind is > 8 m s^{-1} in most of this period (Figure 2c). Friction velocity becomes sufficiently

456   high to overcome the gravity and bonds between snow particles in this strong wind and raise the

457   snow particles from the surface (van den Broeke et al., 2006; Thiery et al., 2012; Tanji et al., 2021).

458 However, the mean surface wind in ERA5 is convergent around the observation site during the

459 intense wind period (Figure 8), which might not be expected for snow depth to decrease due to

460 snowdrift. The coarse resolution of the atmospheric reanalysis might not produce a realistic surface

461 wind field, which is primarily determined by the local topography (Van Den Broeke et al., 1999;

462 Frezzotti et al., 2005). In addition, surface sublimation of drifting snow particles, which is most

463 significant in warm, dry, and windy weather (Thiery et al., 2012), plays an important role in surface

464 mass balance (Van den Broeke et al., 2004) but has not been involved in ICEPACK yet.

465
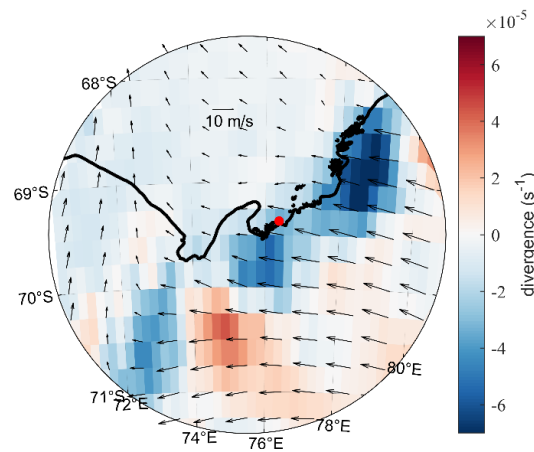
466 Figure 8 The mean ERA5 surface wind and divergence from August 2 to 10. The black line
467 represents the coastline, and the red point represents the observation site.

468

5 Discussions

470 The surface wind can affect the snow depth by changing the surface heat fluxes (Fairall et al.,

471 2003). Compared with Sim_Obs, Sim_ERA_W gives a -2.5×10^4 W m^{-2} lower latent heat flux

472 (positive downward) on average (Figure 9b), i.e., a larger sublimation (Figure 9c), and a reduction

473 of about -3.4 cm of the snow depth (Figure 9a). Therefore, the overestimation in the surface wind

474 from ERA5 partly neutralizes the effect of overestimated precipitation.

475

476
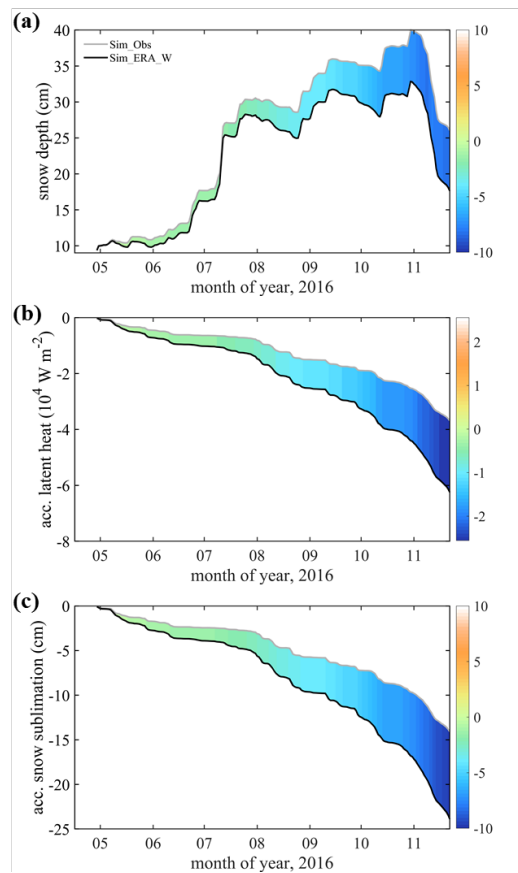
Figure 9 Times series of (a) snow depth, (b) accumulated latent heat flux, and (c) accumulated snow

sublimation. The gray line represents the simulation using wind from the observation (Sim_Obs).

The black line represents the simulation using wind from ERA5 (Sim_ERA_W). The color bar

represents their difference (Sim_ERA_W – Sim_Obs).

The oceanic forcing also plays an essential role in sea ice evolution (Uotila et al., 2019). Heat

flux from the ocean boundary layer changes the sea ice energy balance (Maykut and Untersteiner,

1971). The ocean heat flux is mainly impacted by summer insolation through open leads, thin ice,

melt ponds (Perovich and Maykut, 1990), and upward heat transfer through vertical turbulent

mixing (McPhee et al., 1999). Because the oceanic observations under sea ice are challenging, most

sea ice models directly use some empirical values, like the default value in CCSM3, to build the

ocean boundary condition (e.g., Yang et al., 2016b; Turner and Hunke, 2015). ~~In this study, although~~

~~some oceanic variables, like the water temperature and salinity, are from observation, while others,~~

~~like the mixed layer depth, simply refers~~ Although some oceanic variables, like the water

temperature and salinity, are from observation, others refer to previous studies, like the mixed layer

depth ~~to previous studies~~. The uncertainty in oceanic forcing might be as important as the

492 atmospheric ones, which will be focused on in our coming work.

493

6 Conclusions

495 This work uses the single-column sea ice model ICEPACK forced by the ERA5 atmospheric

496 reanalysis and atmospheric *in situ* observations to simulate snow depth and sea ice thickness at

497 Zhongshan Station, Antarctic. ~~The main results are listed below:~~We find that

498 ~~f~~Forc~~ing~~ed by atmospheric variables from *in situ* observations~~, t~~. The ICEPACK can ~~well~~

499 reasonably simulate the sea ice thickness evolution but significantly overestimates the snow depth

500 after the ~~11th July precipitation event~~heavy snowfall on July 11. ~~This is because the model does not~~

501 ~~include the snowdrift process.~~ When using atmospheric forcing from ERA5, sea ice thickness

502 simulation is close to observation before July 11~~,~~ but ~~then~~ suddenly increases after~~in the~~~~an extremely~~

503 ~~large precipitation~~snowfall event.

504 ~~We have done~~From the sensitivity experiments, we find that the significant deviation in the

505 precipitation of ERA5 contribute to the largest bias in both sea ice thickness and snow depth even

506 though the precipitation is moderately sensitive to sea ice thickness (-0.032 cm/%) and snow depth

507 (0.135 cm/%). On average, about 2 mm day^{-1} more precipitation in ERA5 is found during the

508 observation period, which produces about 14.5 cm excess in sea ice thickness and 17.3 cm more

509 snow depth.

510 ~~(1)~~We further explore the physical mechanism of the effect of precipitation on ice thickness.

511 Snow-ice formation can be triggered by a heavy snowfall episode, like on July 11. It efficiently

512 produces ice at the sea ice surface, decelerates the snow accumulation, and inhibits sea ice's

513 basal growth. When the snowfall is weak, the snow layer thickens quickly and hampers the sea

514 ice growth through its insulation effect. When the snowfall increases to a certain degree (~1 mm

515 day^{-1}), it will trigger a continuous flooding process, accelerating the sea ice growth and slowing

516 down the snow layer thickening. ~~For the entire simulation period, ERA5 obviously causes an~~

517 ~~overestimation in snow depth compared to observation.~~

518 ~~(2)Although sea ice sensitivity (-0.032 cm/%) is small and snow thickness sensitivity (0.135~~

519 ~~cm/%) is moderate to precipitation in ICEPACK, the significant deviation in the reanalysis's~~

520 ~~precipitation contribute to the largest bias in both sea ice thickness and snow depth. On average,~~

521 ~~about 2 mm day^{-1} more precipitation in ERA5 is found during the observation period, which~~

522 ~~produces about 14.5 cm excess in sea ice thickness and 17.3 cm more snow depth.~~

523 ~~(3) The flooding process can be triggered by a heavy snowfall episode, like on July 11. It~~

524 ~~efficiently produces ice at the sea ice surface, decelerates the snow accumulation, and inhibits~~

525 ~~sea ice's basal growth.~~

526 ~~(4)~~(1)   ~~The interaction between sea ice and its covering snow determines their~~

527 ~~response to snowfall. When the snowfall is weak, the snow layer thickens quickly and hampers~~

528 ~~the sea ice growth through its insulation effect. When the snowfall increases to a certain degree~~

529 ~~(~1 mm day^{-1}), it will trigger a continuous flooding process, accelerating the sea ice growth and~~

530 ~~slowing down the snow layer thickening.~~

531

Acknowledgments

533 The authors would like to thank ECMWF for the ERA5 reanalysis data set and the Russian
534 meteorological station Progress II for the precipitation observations. We are grateful to CICE
535 Consortium for sharing ICEPACK and its documentation (https://github.com/CICE-
536 Consortium/Icepack). This study is supported by the National Natural Science Foundation of China
537 (No. 41941009, 41922044), the Guangdong Basic and Applied Basic Research Foundation (No.
538 2020B1515020025), the Southern Marine Science and Engineering Guangdong Laboratory (Zhuhai)
539 (No. SML2020SP007), and CAS "Light of West China" Program (No. E129030101, Y929641001).
540 PH was supported by AAS grant 4506.

References

542 Barthélemy, A., Goosse, H., Fichefet, T., and Lecomte, O.: On the sensitivity of Antarctic sea ice model
543 biases to atmospheric forcing uncertainties, Clim. Dynam., 51, 1585-1603, 2018.

544 Bitz, C. M., Holland, M. M., Weaver, A. J., and Eby, M.: Simulating the ice‐thickness distribution in a
545 coupled climate model, Journal of Geophysical Research: Oceans, 106, 2441-2463, 2001.

546 Bracegirdle, T. J., and Marshall, G. J.: The reliability of Antarctic tropospheric pressure and temperature
547 in the latest global reanalyses, J. Climate, 25, 7138-7146, 2012.

548 Briegleb, B. P., and Light, B.: A Delta-Eddington multiple scattering parameterization for solar radiation
549 in the sea ice component of the Community Climate System Model, NCAR Tech. Note NCAR/TN-472+
550 STR, 1-108, 2007.

551 Bromwich, D. H., Fogt, R. L., Hodges, K. I., and Walsh, J. E.: A tropospheric assessment of the ERA‐
552 40, NCEP, and JRA‐25 global reanalyses in the polar regions, Journal of Geophysical Research:
553 Atmospheres, 112, D10111, 2007.

554 Chemke, R., and Polvani, L. M.: Using multiple large ensembles to elucidate the discrepancy between
555 the 1979–2019 modeled and observed Antarctic sea ice trends, Geophys. Res. Lett., 47, e2020G-
556 e88339G, 2020.

557 Cheng, B., Mäkynen, M., Similä, M., Rontu, L., and Vihma, T.: Modelling snow and ice thickness in the
558 coastal Kara Sea, Russian Arctic, Ann. Glaciol., 54, 105-113, 2013.

559 Cheng, B., Zhang, Z., Vihma, T., Johansson, M., Bian, L., Li, Z., and Wu, H.: Model experiments on

snow and ice thermodynamics in the Arctic Ocean with CHINARE 2003 data, Journal of Geophysical Research: Oceans, 113, C9020, 2008.

Collins, W. D., Bitz, C. M., Blackmon, M. L., Bonan, G. B., Bretherton, C. S., Carton, J. A., Chang, P., Doney, S. C., Hack, J. J., and Henderson, T. B.: The community climate system model version 3 (CCSM3), J. Climate, 19, 2122-2143, 2006.

Fairall, C. W., Bradley, E. F., Hare, J. E., Grachev, A. A., and Edson, J. B.: Bulk parameterization of air–sea fluxes: Updates and verification for the COARE algorithm, J. Climate, 16, 571-591, 2003.

Fréville, H., Brun, E., Picard, G., Tatarinova, N., Arnaud, L., Lanconelli, C., Reijmer, C., and Van den Broeke, M.: Using MODIS land surface temperatures and the Crocus snow model to understand the warm bias of ERA-Interim reanalyses at the surface in Antarctica, The Cryosphere, 8, 1361-1373, 2014.

Frezzotti, M., Pourchet, M., Flora, O., Gandolfi, S., Gay, M., Urbini, S., Vincent, C., Becagli, S., Gragnani, R., and Proposito, M.: Spatial and temporal variability of snow accumulation in East Antarctica from traverse data, J. Glaciol., 51, 113-124, 2005.

Gascoin, S., Lhermitte, S., Kinnard, C., Bortels, K., and Liston, G. E.: Wind effects on snow cover in Pascua-Lama, Dry Andes of Chile, Adv. Water Resour., 55, 25-39, 2013.

Granskog, M. A., Leppäranta, M., Kawamura, T., Ehn, J., and Shirasawa, K.: Seasonal development of the properties and composition of landfast sea ice in the Gulf of Finland, the Baltic Sea, Journal of Geophysical Research: Oceans, 109, 10.1029/2003JC001874, 2004.

Hao, G., Pirazzini, R., Yang, Q., Tian, Z., and Liu, C.: Spectral albedo of coastal landfast sea ice in Prydz Bay, Antarctica, J. Glaciol., 67, 1-11, 2020.

Hao, G., Yang, Q., Zhao, J., Deng, X., Yang, Y., Duan, P., Zhang, L., Li, C., and Cui, L.: Observation and analysis of landfast ice arounding Zhongshan Station, Antarctic in 2016, Haiyang Xuebao, 9, 26-39, 2019.

Heil, P.: Atmospheric conditions and fast ice at Davis, East Antarctica: A case study, Journal of Geophysical Research: Oceans, 111, C5009, 2006.

Heil, P., Allison, I., and Lytle, V. I.: Seasonal and interannual variations of the oceanic heat flux under a landfast Antarctic sea ice cover, Journal of Geophysical Research: Oceans, 101, 25741-25752, 1996.

Hersbach, H., Bell, B., Berrisford, P., Hirahara, S., Horányi, A., Muñoz Sabater, J., Nicolas, J., Peubey, C., Radu, R., and Schepers, D.: The ERA5 global reanalysis, Q. J. Roy. Meteor. Soc., 146, 1999-2049, 2020.

Hersbach, H., and Dee, D.: ERA5 reanalysis is in production, ECMWF Newsletter 147, Reading, UK: ECMWF. [Retrieved from https://www. ecmwf. int/en/newsletter/147/news/era5-reanalysis-production], 2016.

Hunke, E., Allard, R., Bailey, D. A., Blain, P., Craig, T., Dupont, F., DuVivier, A., Grumbine, R., Hebert, D., Holland, M., Jeffery, N., Lemieux, J., Rasmussen, T., Ribergaard, M., Roberts, A., Turner, M., and Winton, M.: CICE-Consortium/Icepack: Icepack1.1.1, doi:10.5281/zenodo.3251032, 2019.

Jakobs, C. L., Reijmer, C. H., Smeets, C. P., Trusel, L. D., Van De Berg, W. J., Van Den Broeke, M. R., and Van Wessem, J. M.: A benchmark dataset of in situ Antarctic surface melt rates and energy balance, J. Glaciol., 66, 291-302, 2020.

Jeffries, M. O., Krouse, H. R., Hurst-Cushing, B., and Maksym, T.: Snow-ice accretion and snow-cover depletion on Antarctic first-year sea-ice floes, Ann. Glaciol., 33, 51-60, DOI: 10.3189/172756401781818266, 2001.

Jones, R. W., Renfrew, I. A., Orr, A., Webber, B., Holland, D. M., and Lazzara, M. A.: Evaluation of four global reanalysis products using in situ observations in the Amundsen Sea Embayment, Antarctica,

Journal of Geophysical Research: Atmospheres, 121, 6240-6257, 2016.

Kawamura, T., Ohshima, K. I., Takizawa, T., and Ushio, S.: Physical, structural, and isotopic characteristics and growth processes of fast sea ice in Lützow-Holm Bay, Antarctica, Journal of Geophysical Research: Oceans, 102, 3345-3355, 10.1029/96JC03206, 1997.

Krumpen, T., Birrien, F., Kauker, F., Rackow, T., Albedyll, L. V., Angelopoulos, M., Belter, H. J., Bessonov, V., Damm, E., and Dethloff, K.: The MOSAiC ice floe: sediment-laden survivor from the Siberian shelf, The Cryosphere, 14, 2173-2187, 2020.

Lei, R., Li, Z., Cheng, B., Zhang, Z., and Heil, P.: Annual cycle of landfast sea ice in Prydz Bay, east Antarctica, Journal of Geophysical Research: Oceans, 115, C2006, 2010.

Leppäranta, M.: A growth model for black ice, snow ice and snow thickness in subarctic basins, Hydrology Research, 14, 59-70, 1983.

Lindsay, R., Wensnahan, M., Schweiger, A., and Zhang, J.: Evaluation of seven different atmospheric reanalysis products in the Arctic, J. Climate, 27, 2588-2606, 2014.

Lindsay, R., and Schweiger, A.: Arctic sea ice thickness loss determined using subsurface, aircraft, and satellite observations, The Cryosphere, 9, 269-283, 2015.

Liston, G. E., Polashenski, C., Rösel, A., Itkin, P., King, J., Merkouriadi, I., and Haapala, J.: A distributed snow‐evolution model for sea‐ice applications (SnowModel), Journal of Geophysical Research: Oceans, 123, 3786-3810, 2018.

Liu, C., Gao, Z., Yang, Q., Han, B., Wang, H., Hao, G., Zhao, J., You, L., Yang, Y., Wang, L., Li, Y.: Observed surface fluxes over sea ice near Antarctic Zhongshan station from April to November in 2016, Annals of Glaciology, 61(82) ,12-23, 2020.

Liu, C., Hao, G., Li, Y., Zhao, J., Lei, R., Cheng, B., Gao, Z., Yang, Q.: The sensitivity of parameterization schemes in thermodynamic modeling of the landfast sea ice in Prydz Bay, East Antarctica, Journal of Glaciology, 1-16, 2022.

Massom, R. A., Eicken, H., Hass, C., Jeffries, M. O., Drinkwater, M. R., Sturm, M., Worby, A. P., Wu, X., Lytle, V. I., and Ushio, S.: Snow on Antarctic sea ice, Rev. Geophys., 39, 413-445, 2001.

Massonnet, F., Fichefet, T., Goosse, H., Vancoppenolle, M., Mathiot, P., and König Beatty, C.: On the influence of model physics on simulations of Arctic and Antarctic sea ice, The Cryosphere, 5, 687-699, 2011.

Maykut, G. A., and Untersteiner, N.: Some results from a time-dependent thermodynamic model of sea ice, Journal of Geophysical Research (1896-1977), 76, 1550-1575, 10.1029/JC076i006p01550, 1971.

Maykut, G. A., and McPhee, M. G.: Solar heating of the Arctic mixed layer, Journal of Geophysical Research: Oceans, 100, 24691-24703, 1995.

McPhee, M. G., Kottmeier, C., and Morison, J. H.: Ocean Heat Flux in the Central Weddell Sea during Winter, J. Phys. Oceanogr., 29, 1166-1179, 10.1175/1520-0485(1999)029<1166:OHFITC>2.0.CO;2, 1999.

Merkouriadi, I., Liston, G. E., Graham, R. M., and Granskog, M. A.: Quantifying the potential for snow‐ice formation in the Arctic Ocean, Geophys. Res. Lett., 47, e2019G-e85020G, 2020.

Parkinson, C. L.: A 40-y record reveals gradual Antarctic sea ice increases followed by decreases at rates far exceeding the rates seen in the Arctic, Proceedings of the National Academy of Sciences, 116, 14414-14423, 2019.

Parkinson, C. L., and Cavalieri, D. J.: Antarctic sea ice variability and trends, 1979-2010, The Cryosphere, 6, 871-880, 2012.

Perovich, D. K., and Maykut, G. A.: Solar heating of a stratified ocean in the presence of a static ice

648 cover, Journal of Geophysical Research: Oceans, 95, 18233-18245, 10.1029/JC095iC10p18233, 1990.

649 Provost, C., Sennéchael, N., Miguet, J., Itkin, P., Rösel, A., Koenig, Z., Villacieros Robineau, N., and

650 Granskog, M. A.: Observations of flooding and snow‐ice formation in a thinner Arctic sea‐ice regime

651 during the N‐ICE2015 campaign: Influence of basal ice melt and storms, Journal of Geophysical

652 Research: Oceans, 122, 7115-7134, 2017.

653 Roussel, M., Lemonnier, F., Genthon, C., and Krinner, G.: Brief communication: Evaluating Antarctic

654 precipitation in ERA5 and CMIP6 against CloudSat observations, The Cryosphere, 14, 2715-2727, 2020.

655 Saloranta, T. M.: Modeling the evolution of snow, snow ice and ice in the Baltic Sea, Tellus A: Dynamic

656 Meteorology and Oceanography, 52, 93-108, 2000.

657 Schlosser, E., Haumann, F. A., and Raphael, M. N.: Atmospheric influences on the anomalous 2016

658 Antarctic sea ice decay, The Cryosphere, 12, 1103-1119, 2018.

659 Stroeve, J. C., Serreze, M. C., Holland, M. M., Kay, J. E., Malanik, J., and Barrett, A. P.: The Arctic's

660 rapidly shrinking sea ice cover: a research synthesis, Climatic Change, 110, 1005-1027, 2012.

661 Stuecker, M. F., Bitz, C. M., and Armour, K. C.: Conditions leading to the unprecedented low Antarctic

662 sea ice extent during the 2016 austral spring season, Geophys. Res. Lett., 44, 9008-9019, 2017.

663 Tanji, S., Inatsu, M., and Okaze, T.: Development of a snowdrift model with the lattice Boltzmann

664 method, Progress in Earth and Planetary Science, 8, 1-16, 2021.

665 Tetzner, D., Thomas, E., and Allen, C.: A Validation of ERA5 Reanalysis Data in the Southern Antarctic

666 Peninsula—Ellsworth Land Region, and Its Implications for Ice Core Studies, Geosciences, 9, 289, 2019.

667 Thiery, W., Gorodetskaya, I. V., Bintanja, R., Van Lipzig, N., Van den Broeke, M. R., Reijmer, C. H.,

668 and Kuipers Munneke, P.: Surface and snowdrift sublimation at Princess Elisabeth station, East

669 Antarctica, The Cryosphere, 6, 841-857, 2012.

670 Tsamados, M., Feltham, D. L., and Wilchinsky, A. V.: Impact of a new anisotropic rheology on

671 simulations of Arctic sea ice, Journal of Geophysical Research: Oceans, 118, 91-107, 2013.

672 Turner, A. K., Hunke, E. C., and Bitz, C. M.: Two modes of sea-ice gravity drainage: A parameterization

673 for large‐scale modeling, Journal of Geophysical Research: Oceans, 118, 2279-2294, 2013.

674 Turner, A. K., and Hunke, E. C.: Impacts of a mushy-layer thermodynamic approach in global sea-ice

675 simulations using the CICE sea-ice model, Journal of Geophysical Research: Oceans, 120, 1253-1275,

676 2015.

677 Turner, J., Phillips, T., Marshall, G. J., Hosking, J. S., Pope, J. O., Bracegirdle, T. J., and Deb, P.:

678 Unprecedented springtime retreat of Antarctic sea ice in 2016, Geophys. Res. Lett., 44, 6868-6875,

679 2017.Uotila, P., Goosse, H., Haines, K., Chevallier, M., Barthélemy, A., Bricaud, C., Carton, J., Fučkar,

680 N., Garric, G., and Iovino, D.: An assessment of ten ocean reanalyses in the polar regions, Clim. Dynam.,

681 52, 1613-1650, 2019.

682 Urraca, R., Huld, T., Gracia-Amillo, A., Martinez-de-Pison, F. J., Kaspar, F., and Sanz-Garcia, A.:

683 Evaluation of global horizontal irradiance estimates from ERA5 and COSMO-REA6 reanalyses using

684 ground and satellite-based data, Sol. Energy, 164, 339-354, 2018.

685 Van Den Broeke, M. R., Winther, J., Isaksson, E., Pinglot, J. F., Karlöf, L., Eiken, T., and Conrads, L.:

686 Climate variables along a traverse line in Dronning Maud Land, East Antarctica, J. Glaciol., 45, 295-302,

687 1999.

688 Van Den Broeke, M. R., Reijmer, C. H., and Van De Wal, R. S.: A study of the surface mass balance

689 in Dronning Maud Land, Antarctica, using automatic weather stations, J. Glaciol., 50, 565-582, 2004.

690 Van Den Broeke, M., Reijmer, C., and Van De Wal, R.: Surface radiation balance in Antarctica as

691 measured with automatic weather stations, Journal of Geophysical Research: Atmospheres, 109, 2004.

Vancoppenolle, M., Timmermann, R., Ackley, S. F., Fichefet, T., Goosse, H., Heil, P., Leonard, K. C., Lieser, J., Nicolaus, M., and Papakyriakou, T.: Assessment of radiation forcing data sets for large-scale sea ice models in the Southern Ocean, Deep Sea Research Part II: Topical Studies in Oceanography, 58, 1237-1249, 2011.

Vignon, É., Traullé, O., and Berne, A.: On the fine vertical structure of the low troposphere over the coastal margins of East Antarctica, Atmos. Chem. Phys., 19, 4659-4683, 2019.

Wang, C., Graham, R. M., Wang, K., Gerland, S., and Granskog, M. A.: Comparison of ERA5 and ERA-Interim near-surface air temperature, snowfall and precipitation over Arctic sea ice: effects on sea ice thermodynamics and evolution, The Cryosphere, 13, 1661-1679, 2019b.

Wang, G., Hendon, H. H., Arblaster, J. M., Lim, E., Abhik, S., and van Rensch, P.: Compounding tropical and stratospheric forcing of the record low Antarctic sea-ice in 2016, Nat. Commun., 10, 1-9, 2019a.

Wang, Y., Zhou, D., Bunde, A., and Havlin, S.: Testing reanalysis data sets in Antarctica: Trends, persistence properties, and trend significance, Journal of Geophysical Research: Atmospheres, 121, 12-839, 2016.

Yang, Q., Liu, J., Leppäranta, M., Sun, Q., Li, R., Zhang, L., Jung, T., Lei, R., Zhang, Z., and Li, M.: Albedo of coastal landfast sea ice in Prydz Bay, Antarctica: Observations and parameterization, Adv. Atmos. Sci., 33, 535-543, 2016a.

Yang, Y., Zhijun, L., Leppäranta, M., Cheng, B., Shi, L., and Lei, R.: Modelling the thickness of landfast sea ice in Prydz Bay, East Antarctica, Antarct. Sci., 28, 59-70, 2016b.

Zhang, J.: Increasing Antarctic sea ice under warming atmospheric and oceanic conditions, J. Climate, 20, 2515-2529, 2007.

Zhang, J.: Modeling the impact of wind intensification on Antarctic sea ice volume, J. Climate, 27, 202-214, 2014.

Zhao, J., Cheng, B., Yang, Q., Vihma, T., and Zhang, L.: Observations and modelling of first-year ice growth and simultaneous second-year ice ablation in the Prydz Bay, East Antarctica, Ann. Glaciol., 58, 59-67, 2017.

Zhao, J., Cheng, B., Vihma, T., Yang, Q., Hui, F., Zhao, B., Hao, G., Shen, H., and Zhang, L.: Observation and thermodynamic modeling of the influence of snow cover on landfast sea ice thickness in Prydz Bay, East Antarctica, Cold Reg. Sci. Technol., 168, 102869, 2019.